ON THE NUMERICAL INVESTIGATION OF INLET BUZZ FLOW

Pong-Jeu Lu and Ling-Tzong Jain
Institute of Aeronautics and Astronautics
National Cheng Kung University, Taiwan, China

Abstract

The present research aims at developing a high-resolution total variation diminishing (TVD) scheme and a data processing procedure that can solve the inlet buzz flow problem. A 10 ft. ramjet engine used by Dailey was adopted as the simulation model. The results show that the buzz cycle is attributed both to the local flow instability around the entrance and to the acoustic resonance modes appearing inside the plenum chamber. A revised upstream feedback mechanism is proposed in the present work. It was found that the feedback loop for the subcritical operation is established locally around the inlet region, and the feedback acoustic waves were sent upstream by the impingement of the shock-induced separation vorticities on the center-body surface and/or the cowl lip. For the supercritical operation, however, the formation of the feedback mechanism is ascribed to the fundamental acoustic resonance mode generated in the plenum chamber.

Introduction

Supersonic inlet is designed to efficiently reduce the flow velocity relative to the engine so that the burning in the combustion chamber may remain stable. However, experiences show that the undesired buzz phenomenon may sometimes arise in the subcritical operation condition, significantly deteriorating the propulsion system performance due to the resulting combustion instability, engine surge, thrust loss, etc. A serious buzz phenomenon can even lead to the destruction of the engine. Although the buzz phenomenon has been known since the early design of the ramjet engine,[1] the physical characteristics involved have yet been thoroughly understood. The explanation of the physical mechanism was based primarily on the observations obtained from the very limited experimental measurements,[2-4] and the theoretical analyses,[5,6] basically, were highly idealized which failed to give a precise account of the entire physical pictures.

Inlet buzz can be categorized as one of the many self-excited flows that occur in the fluid dynamics. Excellent reviews on the self-excited flows[7-9] are available. In general, the incompressible or the low-speed self-excited flows are comparatively better understood than those of the high-speed flows. It is generally agreed that a self-excited flow must be formed in a closed-loop manner, which consists mainly of two mutually interactive elements, i.e., an instability origin and the associated downstream propagated instability wave, and an upstream feedback mechanism. The acoustic wave often plays the role of the upstream feedback mechanism since the entropy and vorticity waves are convective waves that flow downstream with the stream. In the presently interested supersonic inlet flow, all these basic elements and their interactions become not so clearly defined; the origin of the instability wave (the shock-induced separation point) is moving, the sources of the upstream propagated acoustic wave are hard to define, and how the acoustic resonance of the internal flow affects the system dynamics is not fully understood, leading to a situation which is very difficult to be analyzed in a straightforward way.

Buzz phenomena are generally categorized into two types; the so-called Dailey-type[3] and Ferri-type.[2] Dailey-type, which is the main concern of the present study, is typified by the center-body flow separation and its interaction with the duct acoustic resonance. The present work attempts to analyze this Dailey inlet buzz flow numerically. Advantage will be taken of the abundant data obtained in the simulations. The underlying physics will be disclosed using various data processing techniques in conjunction with the available experimental results.

The Navier-Stokes computations concerning the unsteady inlet buzz flow were first conducted by Newsome[10] using the MacCormack explicit scheme. Buzz flow was obtained only for the closed-end case in which the traveling shock and the high-frequency oscillation were seen. Unfortunately, the computed high-frequency oscillation was found to be associated with the first duct acoustic mode (f=127 Hz), contrary to the experimental result of the third mode (f=391 Hz). The reason for this frequency mismatch of the numerical and experimental results was not explained. Moreover, there exists no detailed data analysis to justify how waves may interact and why buzz flow was not observed for the near-critical numerical simulation case, while a

110 Hz high-frequency flow oscillation was observed in the experiment.

Shigematsu[11] also performed an inlet flow calculation, by making use of a flow plug in the rear of a two-dimensional ramjet to facilitate the control of the back pressure and the mass flux. Numerical results showed reasonably good prediction of the center-body surface pressure distributions as compared to the experimental data. As the flow plug is largely closed, buzz flow was observed in the experiment whereas there were no comments made about the corresponding numerical simulation. Unsteady inlet flow phenomena were reported occurring in the simulation, however, there existed no accompanying experimental data to compare with. The correctness of the numerical simulation, in particular the unsteady flows, hence cannot be evaluated properly.

The raised numerical simulations of inlet buzz flow indicate that analyzing buzz flow by means of numerical approach is promising but immature. There still exists room for the improvements on the numerical scheme and the procedure of buzz flow initiation. The Dailey's experiment, to the knowledge of the authors, is the most thorough work on inlet buzz that can be found in the open literature. It is this reason that Dailey's work was presently re-investigated numerically. Critical numerical procedures leading to the buzz flow condition were carefully examined first. The buzz flow simulations were then performed with the computed results checked satisfactorily with the experimental data, and a revised buzz flow mechanism was proposed based on these numerical evidences observed.

Numerical Methods

Governing Equations

In the inlet flow simulations, experiences show that viscous effects are very important. This is because that the boundary layer effects and the flow separation phenomenon are very influential on the internal flow developments. Hence, the Reynolds-averaged Navier-Stokes equations are presently adopted as the governing equations to be simulated. The governing equations can be written in a compact integral form for an axi-symmetric flow as:

$$\frac{\partial}{\partial t}\int_V Q dV + \oint_S n\cdot \mathbf{F}\, dS = \oint_S n\cdot \mathbf{F_V}\, dS + \int_V H dS \qquad (1)$$

in which the variables V and S are the control volume and the control surface, respectively; and the conservation variables Q are defined by

$$Q = \begin{pmatrix} e \\ \rho \\ \rho u \\ \rho v \end{pmatrix} \qquad (2)$$

where e is the internal energy, ρ the density, u and v are the velocity components in the Cartesian x and y directions in the symmetry plane. The convective and viscous flux terms $\mathbf{F}$ and $\mathbf{F_V}$ are defined respectively by the column vectors

$$\mathbf{F} = E\vec{i} + F\vec{j}, \quad \mathbf{F_V} = E_v\vec{i} + F_v\vec{j} \qquad (3)$$

The convective fluxes, E, F are the components of the flux vector, $\mathbf{F}$, in the x and y directions, which can be expressed as:

$$E = \begin{pmatrix} e(u-u_g)+pu \\ \rho(u-u_g) \\ \rho u(u-u_g)+p \\ \rho(u-u_g)v \end{pmatrix}, \quad F = \begin{pmatrix} e(v-v_g)+pv \\ \rho(v-v_g) \\ \rho v(v-v_g) \\ \rho v(v-v_g)+p \end{pmatrix} \qquad (4)$$

In the above notations, p is the static pressure, u_g, v_g are the control surface boundary velocity components. These control surface velocity terms are required when dynamic mesh system is used for generating the buzz flow. The mesh movement, hence the cell velocity $V_g(=u_g\vec{i}+v_g\vec{j})$, ought to satisfy the geometric conservation law:[12]

$$\frac{\partial}{\partial t}\int_V dV + \oint n\cdot V_g\, dS = 0 \qquad (5)$$

The definitions of the viscous fluxes and the source term H appearing on the right hand side of Eq.(1) can be found in Ref. 13. To close up the above Navier-Stokes equations, the following thermodynamic equation of state is used,

$$p = (\gamma-1)\left[e - \frac{1}{2}\rho(u^2+v^2)\right] \qquad (6)$$

The viscosity is assumed to be temperature dependent only, defined using the Sutherland's equation,

$$\frac{\mu}{\mu_\infty} = \frac{T_\infty + 198.6}{T + 198.6}\left(\frac{T}{T_\infty}\right)^{3/2} \tag{7}$$

By an appropriate non-dimensionalization (i.e., using a representative length scale l of the flowfield, the freestream sound speed c_∞ as the reference velocity, and a time scale l/c_∞, and note that the density ρ and viscosity μ can be non-dimensionalized by their freestream values, and the pressure p and internal energy e by $\rho_\infty c_\infty^2$, respectively), Eq.(1) can be rewritten in the original form except that the viscous fluxes E_v and F_v are modified (see Ref.13 for the nomenclature):

$$E_v = \frac{1}{\mathrm{Re}}\begin{pmatrix} \frac{\mu}{\mathrm{Pr}}T_x + u\sigma_{xx} + v\sigma_{xy} \\ 0 \\ \sigma_{yx} \\ \sigma_{yy} \end{pmatrix}$$

$$F_v = \frac{1}{\mathrm{Re}}\begin{pmatrix} \frac{\mu}{\mathrm{Pr}}T_y + u\sigma_{yx} + v\sigma_{yy} \\ 0 \\ \sigma_{yx} \\ \sigma_{yy} \end{pmatrix} \tag{8}$$

in which, the Reynolds and Prandtl numbers and the normalized viscosity are defined respectively by

$$\mathrm{Re} = \frac{\rho_\infty l c_\infty}{\mu_\infty}, \qquad \mathrm{Pr} = \frac{C_p \mu}{k}, \qquad \mu = \frac{\mu}{\mu_\infty} \tag{9}$$

Since for separated flow with strong pressure gradient there is no conclusive superiority that can be claimed for using certain turbulence model, we simply used Baldwin-Lomax algebraic model[14] to approximate the turbulence behavior. In our buzz flow tests we even switched off the turbulence model, however, the results showed no significant differences. The problem of turbulence modeling in shock-induced separated flow deserves further studies, nevertheless, it goes beyond the scope of the present research.

Finite-volume Scheme

In the finite-volume approach, the volume integral, Eq. (1), as applied to a finite control volume, $V_{i,j}$, can be written as:

$$\frac{\partial}{\partial t}\int_{V_{i,j}} Q\,dV + \oint_{S_{i,j}} n\cdot\mathbf{F}\,dS = \oint_{S_{i,j}} n\cdot\mathbf{F_V}\,dS + \int_{V_{i,j}} H\,dS \tag{10}$$

Using appropriate spatial discretization, the above equation can be replaced by a semi-discretized equation

$$\frac{\partial}{\partial t}Q_{i,j}V_{i,j} + \sum_{k=1}^{4}\left(\hat{F}^k_{i,j} - \hat{F}^k_{v_{i,j}}\right) = H_{i,j}V_{i,j} \tag{11}$$

where k represents the four surfaces of each cell. Cell-averaged $Q_{i,j}$ is assumed to be located at the cell centroid and, $\hat{F}^k_{i,j}$, $\hat{F}^k_{v_{i,j}}$ are the normal numerical fluxes approximated at the k-th cell boundary.

The spatial accuracy of the finite-volume discretization depends on the construction of the numerical fluxes $\hat{F}^k$ and $\hat{F}^k_v$. In the present study, The modified Osher-Chakravarthy MUSCL type upwind TVD scheme[15] constructed using the Roe splitting[16] is adopted. This scheme was developed in particular for coping with the acoustic wave simulations.[17] The enforcement of this high-resolution scheme on the dynamic grid was also achieved.[18] This newly developed TVD scheme takes into account the grid nonuniformity effect so that the generation of spurious numerical waves can be minimized during computation.[17]

The system of ordinary differential equations, Eq. (11), can be integrated in time using an explicit m-stage Runge-Kutta scheme expressed in the following form,

$$\begin{aligned} \overline{Q}^{(0)} &= \overline{Q}^n \\ \overline{Q}^{(1)} &= \overline{Q}^{(0)} - \alpha_1 \Delta t\, \hat{R}\left(\overline{Q}^{(0)}\right) \\ &\cdots\cdots \\ \overline{Q}^{(m)} &= \overline{Q}^{(0)} - \alpha_1 \Delta t\, \hat{R}\left(\overline{Q}^{(m-1)}\right) \\ \overline{Q}^{(n+1)} &= \overline{Q}^{(m)} \end{aligned} \tag{12}$$

The present study adopts a three-stage scheme[19] using α_1=0.24, α_2=0.5 α_3=1. This strategy has previously been justified to be of second-order accuracy in time while maintaining the TVD property.[19]

Boundary Condition Treatments

For inviscid and viscous wall boundary conditions, usually the wall pressure must be derived from the governing equations subject to the specified wall boundary conditions. Conventionally, the grids are very much clustered in the boundary layer for viscous simulations, therefore, the use of $\partial p/\partial n = 0$ to extrapolate the wall pressure from the inside neighboring cell-centered values is satisfactory. Here in

our buzz flow calculations the boundary layer approximation often does not hold since massive flow separation may occur due to the strong shock/ boundary layer interaction effect. Owing to this fact, the wall pressure distribution, in both viscous and inviscid calculations, was extrapolated using the pressure gradient derived from the momentum equations.

Considering the most general case of a moving wall with surface blowing or suction applied (This can be thought as a ramjet is maneuvering while the surface bleed flow control of the inlet is in action), the transverse pressure gradient $\partial p / \partial \eta$ can be expressed as:[13]

$$\begin{aligned} &\rho\left(\frac{\partial V_n}{\partial \tau} - \eta_{\tau\tau} - u\frac{\partial \eta_x}{\partial \tau} - v\frac{\partial \eta_y}{\partial \tau}\right) + \rho V_t\left(\eta_x u_\xi + \eta_y v_\xi\right) \\ &+ \rho V_n\left(\eta_x u_\eta + \eta_y v_\eta\right) \\ &= -\left[\left(\xi_x\eta_x + \xi_y\eta_y\right)\frac{\partial p}{\partial \eta} + \left(\eta_x^2 + \eta_y^2\right)\frac{\partial p}{\partial \eta}\right] + \left(\eta_x I_u + \eta_y I_v\right) \end{aligned} \tag{13}$$

where (ξ, η) are grid coordinates and I_u, I_v are the viscous terms

$$I_u = \frac{1}{\mathrm{Re}}\left(\frac{\partial}{\partial x}\sigma_{xx} + \frac{\partial}{\partial y}\sigma_{xy}\right) \tag{14}$$

$$I_v = \frac{1}{\mathrm{Re}}\left(\frac{\partial}{\partial x}\sigma_{xy} + \frac{\partial}{\partial y}\sigma_{yy}\right) \tag{15}$$

In Eq.(13), terms associated with the time derivative $\partial / \partial \tau$ come from the unsteady and/or the dynamic grid effect.[18] The normal and tangential controvariant velocities V_n and V_t are given by

$$V_n = \eta_\tau + \eta_x u + \eta_y v, \quad V_t = \xi_\tau + \xi_x u + \xi_y v \tag{16}$$

The case of $V_n \neq 0$ means surface blowing or suction is applied, and the V_t must be extrapolated from inside of the computational domain. As wall Cartesian velocity components are determined using Eq. (16), all the gradient terms of u and v in Eq.(13) can be approximated. Density ρ is usually extrapolated from the interior neighboring cell-centered values. With all the terms in Eq. (13) being properly approximated using appropriate difference formulas, the transverse pressure gradient $\partial p / \partial \eta$ is hence available, and the surface pressure is obtainable using this gradient value and the adjacent cell-centered pressure value.

The inflow and outflow conditions are treated using standard non-reflective characteristic-based boundary condition treatment.[20,21] In the present simulations this consideration of non-reflective boundaries becomes a bit trivial since the inflow is kept supersonic and the outflow, except during the transient start-up stage, is supersonically discharged since the downstream throat is always choked when buzz occurs.

Dailey-type Inlet Buzz Flow

Physical Description

One of the ramjet engines that Dailey used for his buzz flow study is shown in Fig. 1. In Dailey's experiments, the shock on the center-body of the supersonic ramjet engine oscillated when buzz was initiated. The subcritical operation was interrupted when the inlet shock moved upstream to the tip of the center-body. The high-frequency oscillations (the characteristics of low-mass flow period) were observed during the subcritical operation. At the end of this high-frequency oscillations, the inlet shock moved back into the cowl with air ingested at the supercritical rate. In other words, the subcritical operation was initiated by the blockage of the inlet due to the shock-induced flow separation occurring on the center-body ramp, causing the center-body shock expelled upstream to the cone tip and thus deflect the approaching flow away from the cowl lip. During this inlet blockage stage, the downstream air column in the plenum chamber continued to discharge out of the exit nozzle. As the stored mass reduced due to the discharge of the air out from both ends of the engine, the plenum chamber pressure became low and the expelled shock waves moved back into the inlet duct and the supercritical operation took over. The mass flux flowing into the inlet was therefore greater than the exit discharge rate, and the plenum chamber was therefore filled up with pressure built up until the shock was expelled out to the inlet ramp, returning to the initial subcritical operation condition. This explanation was given by Dailey to describe the buzz cycle he observed.

Dailey's experimental investigation was carried out in the fifties. His explanations about the inlet buzz were made based on four pressure transducer measurements and the high-speed schlieren photography. Although detailed flow structures were not available at that time, the correct overall description of the buzz phenomenon was given. Subsequent studies basically followed Dailey's footprints, elaborating mostly on the downstream acoustic resonance effect. As a result, the discrete duct resonance frequencies can be predicted using a one-dimensional model, but no assertion can be made on which natural frequency should be associated with the low-frequency buzz cycle. The reason is understandable, since the unsteady shock-induced separated boundary layer flow around the inlet ramp was too difficult to analyze, making the upstream instability flow part missing in the theoretical modeling of this

acoustic resonance phenomenon.

In the following, a brief introduction of the acoustic resonance modes was given first to explain the role of diffuser plenum chamber on the buzz dynamics. Then numerical simulations of organ-pipe type duct acoustics were performed to shed light on the numerically captured acoustic field. The effects contributed by the inlet flow structures, which were explained using entrance acoustic impedance, were demonstrated in these organ-pipe simulations. Finally, one of the Dailey's ramjet engines was used for computations and data analysis. Discussions on the inlet buzz mechanism were therefore made based on these processed results.

Duct Acoustic Modes

The flow velocity in the diffuser and plenum chamber is low, which allows the use of acoustic equations to be formulated on the basis of a quiescent mean flow. For a one-dimensional, constant cross-sectional pipe, the governing acoustic equation for the perturbation pressure is,

$$\frac{1}{c^2}\frac{\partial^2 p'}{\partial t^2}+\frac{\partial^2 p'}{\partial x^2}=0 \qquad (17)$$

where c is the sound speed, x=0 and x=L correspond respectively to the inlet and exit positions of this pipe.

The downstream exit can be taken as a closed end since flow is choked as buzz occurs. The boundary condition specified at the upstream end usually is not known *a priori*. If the inlet is taken as closed, which models the inlet blockage during the subcritical operation, an infinitely large acoustic impedance should be specified at x=0, and this will result in an even-mode duct resonance frequency,

$$f_n = 2n\frac{C}{4L} \qquad \text{(even mode)} \qquad (18)$$

During the fill-up stage of the Dailey buzz cycle, the entrance impedance is so low that we can use a vanishing impedance condition to approximate it. Using such a boundary conditions specification, an odd-mode resonance frequency takes place

$$f_n = (2n-1)\frac{C}{4L} \qquad \text{(odd mode)} \qquad (19)$$

It is worth mentioning that as the pipe entrance is open to allow fluid flow in and out, the impedance depends on the local flow structures and usually does not vanish. In what way the resonance condition occurs, in fact, depends on the dynamic characteristics of the surrounding flowfield interfaced with the pipe ends. In the text,[22] there are several examples illustrating the resonant, but non-vanishing local impedance, open-end pipes. In those situations, the pipe length L was modified to account for the non-vanishing resonance impedance and a so-called effective length L_{eff} was used to redefine the resonance frequencies. Similar argument holds for the nearly closed-end case where the impedance is large but still finite.

For the inlet buzz flow problem, very complicated flow situation occurs in the upstream. The shock movement and the shock-induced separated vortical flow together make the entrance impedance of the pipe flow hard to predict. Roughly speaking, during the subcritical stage the plenum pressure is high and the velocity is low, yielding a high impedance condition. During the fill-up stage, flow is accelerated into the plenum chamber so that a low impedance may result from the low pressure and high velocity at the entrance of the plenum chamber. This explains why both even and odd modes appear in the spectra of the measured pressure time histories.

This complicated flow structure in the upstream can be lumped into a simple entrance impedance concept as one wishes to analyze the buzz phenomenon via a one-dimensional duct acoustic model. The inclusion of the entrance impedance stresses that the duct acoustic mode analysis should not leave aside the upstream flow dynamics. In the past, the theoretical works all treated the plenum chamber as an independent mechanism that generated even or odd resonance modes. Moreover, the duct modes were taken as responses forced by the turbulent eddies convected from the upstream. It is proposed here that the acoustic analysis should take into account the upstream dynamics. The upstream dynamics enters in through the boundary condition specification, namely the introduction of the inflow impedance. Therefore, in the subsequent organ-pipe buzz flow simulations, the computed acoustic resonance modes will show frequency shifts in comparison with the even and odd resonance frequencies expressed in Eq.s (18) and (19).

Numerical Buzz Flow Simulation

Organ-pipe Simulation

To see whether the high-frequency oscillation can be simulated properly by the present numerical scheme, the same shortened Dailey engine (1.89 ft) was selected as the model to be computed. In Fig. 2. illustrated this pipe configuration, which was the Dailey ramjet engine with center-body removed. The downstream end is closed to represent the low mass flux condition for a subcritical operation. During computations, there were seven pressure histories that were recorded at the locations denoted respectively by T1, T2, ..., and T7 as

sketched in Fig. 2. Note that the cowl lip is sharp and convex, making vortices easy to be shed as flow oscillates around the cowl lip edge. This vorticity shedding effect was noted by Dailey as the forcing source in exciting the duct resonance modes.

It is interesting to know how important this vorticity shedding is on the duct resonance phenomenon. A specially designed numerical experiment was therefore performed, in which the vorticity generation mechanisms were intentionally minimized. First, the inviscid Euler flow model was used to reduce the vortical layer development along the pipe wall. Second, a constant cross-sectional pipe was adopted which can significantly reduce the possibility of flow separation around the cowl lip. Acoustic waves can still be well represented in this inviscid model since acoustic resonance is basically an inviscid phenomenon.

Numerical computations of these two configurations were performed to simulate pipes immersed in a freestream of Mach number 2. The unsteady flows were all started from their corresponding steady-state flows where the downstream ends were open initially. These steady-state pipe flows were all supersonic, and at some instant the exits were suddenly closed and the impulsively generated shocks were seen propagating upstream toward the inlets. For sufficiently long time, the simulations did not reach steady-states, but instead, the flows showed persistently oscillatory motions without decay. The recorded pressure traces (see Figs. 3 and 4) were Fourier transformed and the spectra are shown in Fig.s 5 and 6. It is observed that discrete spikes show up in these spectral diagrams. The two highest peaks, 112.2 Hz and 138.7 Hz, were found corresponding to the Dailey's and the constant cross-sectional pipes, respectively. These are the fundamental frequencies in which each contains the largest portion of the oscillation energy of the flow.

It was found that the lowest oscillation frequencies, 112.2 Hz and 138.7 Hz, are associated with the oscillatory shock motions. Although both these two pipes are identical in length, the excited fundamental and higher harmonics are different, indicating the effects contributed by the surrounding inflow dynamics around the inlet. Dailey's organ-pipe generated much noisy flowfield than did the constant cross-sectional pipe. The much intensified vorticity field around the cowl lip can be reflected from the T2 pressure trace and its spectrum shown respectively in Figs. 3 and 5. Relatively irregular pressure fluctuations recorded around the Dailey's pipe and much stronger side-band spectrum around the resonance peaks are signatures characterizing the turbulence activities associated with the shedding vorticities. The experimental frequency measured by Dailey was 470 Hz, which agrees well with the second peak, 462.8 Hz, of the present simulation shown in Fig. 5.

The results of the constant cross-sectional pipe simulation show closer resemblance to the analytic solutions. Both even and odd resonance modes appear in the spectrum. The disappearance of the high-frequency modes in the downstream is attributed to the numerical dissipation effect.

Some remarks can be drawn from the present organ-pipe flow simulation. First, the present numerical code can resolve sufficiently, although not completely, the acoustic resonance phenomenon in a pipe. this numerical procedure did not separate the inlet dynamics from the downstream acoustic wave motion. In other words, the feedback loop was naturally accounted for in the simulations. As different inlet shapes, hence different inlet dynamics, are involved, it is found that different resonance frequencies appear although equal length organ-pipes are being used. This finding is particularly valuable for the subsequent inlet buzz analysis. In the past, resonance in the diffuser was taken as a forced response. Self-sustained instability was thought established locally in the upstream inlet zone, and the acoustic modes were excited in the diffuser by the downstream propagated separated vortical flow. This concept makes the past analysis can only predict discrete resonance frequencies. However, it cannot make any comments about which mode might connect with the low-frequency buzz oscillations of the entire system. The present simulations clearly improve this shortcoming. It is shown that the surrounding inlet dynamics does contribute in determining the duct resonance frequencies, as revealed from the different resonance frequencies found in the Dailey's and the constant cross-sectional pipes simulations. The communication connecting the complex upstream inlet flow and the downstream duct acoustic oscillations can be fulfilled by way of the inlet impedance specification. The inclusion of the inflow impedance can therefore affect the resonance modes accordingly.

Dailey Buzz Simulation

The 10 ft. ramjet engine used in Dailey's experiment was chosen for the present simulation. The center-body and cowl lip configuration are shown in Fig. 1. To facilitate numerical computations, the exit was changed using a throat to replace the original conical frustum, making the rear part of the simulated configuration into a convergent-divergent nozzle. The engine length, 10 ft., is now defined as the distance between the tip of the center body and the exit nozzle throat. We chose a 41% captured area as the exit throttle condition for the following numerical simulations.

Numerical Buzz Onset Procedures

Based on our own experiences, the start-up of the internal flow computations is touchy which requires careful treatments. For the present self-sustained flow

freestream capture area. During the subcritical operation (stages (a), (b), (j), (k) and (l)), the inlet has been virtually blocked with extremely low inflow mass flux, and recovers back approximately 20% of the capture area mass flux when the supercritical operation (stages (d) to (h)) prevails.

In the present case, shock is seen completely swallowed into the inlet cowl (see snapshot(h)), however, it does not pass through the inlet throat during the supercritical fill-up period. Partly because that a shock cannot stably stay on a convergent part of a duct, and partly due to the continuingly increasing plenum chamber pressure, the shock starts moving upstream as shown in the stages (h) to (j). Subcritical condition is then resumed together with the high-frequency oscillation sets in.

Figures 14 and 15 portray the spatial-temporal mass flux and pressure distributions in a buzz cycle. These diagrams provide a system view, which is a convenience enjoyed by the CFD simulation, for the inlet buzz analysis. Situations in the plenum chamber are relatively smoother than in the inlet center-body region. Very irregular flow oscillations are observed in both the mass flux and the pressure diagrams around the inlet, as characterized by the corrugated distribution surfaces. In the diffuser plenum chamber ($4 \le x \le 10$), a triple-ridged surface distribution is found for both the mass flux and the pressure distributions. This phenomenon, in fact, results from the coexistence of the most dominant first two resonance modes (n=1, 3 and f_1=27.7 Hz, and f_3=83.1 Hz) in the plenum chamber. However, the second mode (n=3) loses its influence whereas the fundamental (n=1) mode takes a commanding control over the shock motion around the inlet region. The exit throat is seen choked and the discharged mass flux shows a pretty steady trend in time. Therefore, during buzz oscillations, the unsteady and turbulent low-frequency mass flux oscillation occurs primarily in the inlet and the center-body region, while the higher duct acoustic harmonics are excited by the separated wake emerged in the downstream plenum chamber.

The Buzz Feedback Loop

In principle, self-sustained flow oscillation cannot arise in a situation where the resultant event does not link with the cause. The way this upstream cause and downstream event communicate, or the establishment of the so-called feedback loop holds a central position in the self-sustained oscillating flow studies. In subsonic fluid flows, acoustic waves often play this role of upstream influence. Generally speaking, aside from the mixing flows, the feedback signals that can result in a self-excited flow must be strong and organized. Sound induced by vortical waves impinging on a solid surface is a typical way of generating those feedback signals.[23] Dailey made a judicious argument about the feedback loop for the inlet buzz experiments that he performed. He concluded that the instability was caused by the local flow condition around the entrance of the inlet. The possibility of considering the exit throat as a place to generate feedback signals was ruled out by a simple time scale argument. Dailey also explained that the low-frequency buzz cycle occurred in response to the fill-up action in the plenum chamber.

To extract these sound sources out from the simulated results, data processing using the fluctuating dilatation field Δ' can be made,

$$\Delta' = \Delta - \bar{\Delta} \tag{20}$$

$$\Delta = \nabla \cdot \vec{V} \tag{21}$$

where Δ denotes the divergence of the instantaneous velocity field $\vec{V}$ and the overbar "−" stands for time average. the intensity of the sound sources in the fluid flow has been shown to be proportional to the fluctuating dilatation field Δ'.[24,25] Here in our buzz flow simulations the period for averaging the time mean value $\bar{\Delta}$ corresponds to the low-frequency (27.7 Hz) mode. Figure 16 shows these fluctuating dilatation Δ' plots of the aforementioned twelve stages. In order to facilitate the contour plotting work, sound sources arising from the shock dipole effect were filtered out. It is observed that strong sound sources were found at the inlet blockage stages, (a) ~ (c), (h) ~ (l), and the late fill-up stage (h) to (i). The oscillatory forward movement of shock wave during the subcritical inlet blockage period was explained due to the local pressure rise around the inlet entrance. Figure 16 justifies this statement by showing that strong sound sources are produced as the separated vortical structures interact with the cowl and the inlet ramp surfaces. These impinging vorticities may work as a strong dipole sound source, and as feedback to interact with the upstream separation point, will result in a closed-loop, self-excited saw-tooth type high-frequency oscillating flow. Moreover, the shock-induced flow separation point cannot stably stay on the ramp surface, making the shock move forward until it reaches the center-body tip.

Note that at stage (h) the downstream vorticity field becomes so weakened that the previously mentioned impinging vorticity induced sound waves almost disappear. The subsequent supercritical fill-up action, and hence the forward shock motion, would not come into existence if there were no other feedback mechanism checked in. It is the plenum chamber fundamental acoustic resonance mode that takes over the role of upstream feedback which resists this fill-up action by generating an expulsive chamber pressure. The massively separated vorticities that revive again, as shown in stage (i), are caused by this pressure expulsion. As separated vorticities enhance and inlet

simulations, we do not want numerical error signals be mistaken for the physical waves travailing back and forth in the engine, in particular when the errors are hard to be expelled or damped out. A way to achieve this purpose is to let the start-up procedure be compatible with the practical physical situations. To this end, three methods were designed, and in the following their detailed descriptions of the initialization procedure and the results are presented.

The first buzz initiation procedure used the dynamic grid method. Steady-state flow with supersonic outflow was first achieved by letting the diffuser throat fully open. Then the exit throat was gradually squeezed until the desired throat area ratio was obtained. Buzz flow was established and the results are shown in Figs. 7 and 8.

The second start-up procedure used the inviscid Euler solver and the same dynamic grid method addressed above. It is interesting to see that a steady-state inviscid flow was generated. The pattern of a normal shock intersecting with an oblique shock agreed qualitatively with the Dailey's experimental observation. Viscous terms were then added while grid system was refined around the wall region. After the introduction of the viscous effect, the unstable buzz motion appeared, showing a self-excited flow with quite consistent buzz frequency and center-body shock structure as compared to the experimental and the first start-up results.

The reason why buzz flow did not arise in the inviscid flow simulation can be anticipated. Since the instability origin, the shock-induced boundary separation point, was not accounted for in the inviscid model. This points out the important role of the viscous effects in the inlet buzz flow simulations.

The third buzz flow initiation method imitated the actual physical situation of a supersonic flow ramming into the engine. The grid system was kept fixed during the course of computation. The outflow boundary condition was enforced strictly by following the characteristic boundary condition treatment. Before the exit throat was choked, the ambient pressure was used as the specified outflow condition. This subsonic outflow condition treatment was only required for the initial transient flow stage. As buzz flow was established and the exit throat become choked, the supersonic exit flow required no exit boundary condition specification.

An examination of the results computed using different start-up procedures shows that, qualitatively, the same buzz flows were obtained. However, the detailed flow oscillations were not identical nor repeatable, implying the turbulence nature was prevailing in these buzz flow structures. The last buzz initiation method took the longest transient time and the downstream signals (e.g. the T5 trace) were mostly damped. The advantage of using dynamic grid technique for starting the numerical buzz computation, therefore, is demonstrated to be economical and reliable.

Buzz Flow Structures

First, let us take a look at the pressure histories recorded at T1, T2, T3 and T5. Figure 9 illustrates the experimental pressure traces measured using pressure transducers. Our numerical results are presented in Fig. 7. The overall impression is that the numerical and experimental results behave in a quite similar manner. (Note that the second experimental pressure measurement was not reliable since the pressure transducer was claimed broken during the course of the experiment). The Fourier spectra of these pressure records are shown in Fig. 8. The lowest resonance mode, which encompasses the largest energy content of the oscillating flow, shows a peak frequency around 27.7 Hz. This value agrees quite closely with the experimentally observed 25 Hz. A number of even and odd modes also show up in Fig. 8. This solution characteristic basically complies with the previous organ-pipe results, which indicates the existence of higher resonance modes in the diffuser flow. Moreover, the broadband spectra were seen to be comparatively intense in the wake region (T3 probe) where vorticity waves were strong.

Shock motion and inlet flow structures are illustrated in Figs. 10 and 11 using a series of Mach number and vorticity snapshots. These contour plots were taken at twelve instants, (a) to (l), as shown in Fig. 12. With the aid of these snapshots, the upstream flow structure and its relationship with the center-body (T1, T2, and T3) and diffuser (T5) pressure trends can be revealed. It is observed that the general buzz flow picture was captured by the present numerical method when comparing these snapshots with the experimental high-speed schlieren photographs.

Stages (a) and (b) represent the moment of serious inlet flow blockage caused by the expelling pressure wave sent from the downstream plenum chamber. The flow blocked and diverged away from the inlet ramp can be seen from the vorticity plots where the shock-induced flow separation is depicted. As shock continues moving upstream to the tip, the air mass is both spilled away from the inlet and exhausted through the exit nozzle. The pressure data recorded at T1, T2 and T3 control points on the center-body are high (see Fig. 12), however, the pressure at the plenum chamber (T5) show a declining trend, indicating that the stored air column, at the inlet block stage, is continuously discharged from the exit nozzle. As the T5 pressure reduces to its minimum (stages(c) -- (d)), the inlet shock can no longer move upstream and starts to accelerate toward the downstream cowl lip. Stages (d) to (h) represent the fill-up period and the T5 pressure trace shows an increasing trend, indicating air mass was compressed and stored. Figure 13 shows the instantaneous mass fluxes at the selected twelve stages, (a) to (l). The vertical coordinate is non-dimensionalized by the mass flux through the

becomes blocked, the local dipole sound sources are strengthened and the local instability loop forms again, as shown in stages (i) to (l).

Hankey[26] collected a number of inlet buzz flows and found that all the buzz frequencies were coincided with the fundamental (n=1) resonance frequencies of the downstream diffuser pipes. This conclusion is also agreed by the present organ-pipe and ramjet buzz flow simulations. To further test the validity of this conclusion, we cut short the present ramjet engine length to 8 ft. Similar buzz behavior has been found. However, the buzz frequency is now increased to 32.5 Hz. Since a shorter pipe length leads to a higher resonance frequency, the latter simulation proves that the low-frequency buzz oscillation must be associated with the pipe acoustic resonance waves. Otherwise, the frequency will not be modified if the buzz is merely a local instability phenomenon around the inlet region. This demonstration shows that the acoustic resonance modes must participate in the formation of the feedback mechanism by coupling with the upstream flow dynamics to result in a buzz instability.

In summary, it is presently proposed that there are two feedback loops contained in the Dailey-type inlet buzz flow. During the subcritical inlet blockage period the instability of the shock motion is caused by the local separated vortical waves and the induced upstream propagating sound generated around the inlet cowl. During the supercritical fill-up stage, the shock excursion is associated with the modulation of the chamber pressure contributed by the fundamental acoustic resonance mode of the diffuser plenum chamber.

Concluding Remarks

Dailey-type inlet buzz flow was revisited using time-accurate Navier-Stokes simulations. A high-resolution modified Osher-Chakravarthy upwind TVD scheme and a finite-volume method were used. Special discussions upon the numerical buzz initiation were made. It was found that the viscous effect plays an essential role in generating the buzz instabilities. Care has been exercised so that the confusion with the numerics can be avoided in the present numerical buzz flow investigation. Successful numerical simulations were achieved with results agreed well with data obtained from the experiments.

A one-dimensional acoustic wave analysis was established, which served as a theoretical background that guided the numerical simulations. This analysis stresses the idea that acoustic resonance is not necessarily an excited response only. Interface impedance, which represents the dynamic effects offered by the surrounding flow, may change the resultant acoustic resonance modes. This closed-loop type view provides valuable guidelines for performing the subsequent numerical data processing and the physical explanations.

Prior to the inlet buzz computations, the organ-pipe oscillatory flow simulations were conducted. The role of vortex shedding from the inlet entrance, and hence the effects provided by the upstream dynamics, were demonstrated. Both the spike-like resonance frequencies and the side-band turbulence excited waves were observed. The results agreed favorably with those of the Dailey's experiment, providing encouraging support for the proposed one-dimensional duct acoustic analysis.

In the last, the Dailey's ramjet engine was used for exploring the underlying inlet buzz mechanism. The computed low-frequency buzz of 27.7 Hz agreed well with the experimentally observed 25 Hz. Contour snapshots, spectral analysis, and technique for extracting the acoustic field have been exploited. All these data processing confirmed and consolidated Dailey's experimental findings and the associated physical explanations.

Dailey was not completely able to explain the role of diffuser resonance in connection with the inlet buzz dynamics. His suggestion that inlet breakdown is a local phenomenon associated with the entrance flow blockage was modified. By the use of fluctuating dilatation field, at different stages, the feedback loops were demonstrated to be generated from the cowl lip and the center-body surface, and from the diffuser plenum chamber as well. These two feedback loops were explained presently as ascribed, respectively, to the different stages pertaining to the subcritical inlet blockage and the supercritical plenum fill-up operations.

References

[1]Oswaititsch, K., "Pressure Recovery in Missiles with Reaction Propulsion at High Supersonic Speeds (The Efficiency of Shock Diffuser)," NACA TM-1140 (translation), June 1947.

[2]Ferri, A. and Nucci, R.M., "The Origin of Aero-dynamic Instability of Supersonic Inlets at Subcritical Conditions," NACA RM-L50K30, Jan. 1951.

[3]Dailey, C. L., "Supersonic Diffuser Instability," Journal of The Aeronautical Sciences, Vol. 22, No. 11, November 1955, pp. 733-749.

[4]Nagashima, T., Obokato, T., and Asanuma, T., "Experiment of Supersonic Air Intake Buzz," Institute of Space and Aeronautical Science, University of Tokyo, Japan, Rept. 481, May 1972.

[5]Mirels, H., "Acoustic Analysis of Ram-Jet Buzz," NACA TM, No. 3574, 1955.

[6]Trimpi, R. L. "A Theory for Stability and Buzz Pulsation Amplitude in Ram Jets and an Experimental Investigation Inducing Scale Effects," NACA Rept. 1265, 1953.

[7]Rockwell, D. and Naudasher, E., "Self-Sustained

1265, 1953.

[7]Rockwell, D. and Naudasher, E., "Self-Sustained Oscillations of Impinging Free Shear Layers," *Annual Review of Fluid Mechanics*, Vol. 11, 1979, pp. 67-94.

[8]Rockwell, D., "Oscillation of Impinging Shear Layers, "*AIAA Journal*, Vol. 21, No.5, May 1983, pp. 645-664.

[9]Meier, G. E., Szumowski, A. P. and Selerowicz, W. C., "Self-Excited Oscillations in Internal Transonic Flows," *Progress of the Aerospace Science*, Vol. 27, 1990, pp. 145-200.

[10]Newsome, R. W., "Numerical Simulation of Near-Critical and Unsteady, Subcritical Inlet Flow," *AIAA Journal*, Vol. 22, No. 10, October 1984, pp. 1375-1379.

[11]Shigematsu, J. and Yamamoto, K., "A Numerical Investigation of Supersonic Inlet Using Implicit TVD Scheme," AIAA Paper No. 90-2135, 1990.

[12]Vinokur, M., "An Analysis of Finite-Difference and Finite-Volume Formulations of Conservation Laws," *Journal of Computational Physics*, Vol. 81, 1989, pp. 1-52.

[13]Jain, L.-T., "On the Numerical Investigation of Inlet Buzz Flow," Ph.D. Dissertation, Institute of Aeronautics and Astronautics, National Cheng Kung University, Tainan, Taiwan, R.O.C., June 1994.

[14]Baldwin, B., and Lomax, H., "Thin Layer Approximation and Algebraic Model of Separated Turbulent Flows," AIAA Paper No. 78-257, 1978.

[15]Chakravarthy, S. R. and Osher, S., "A New Class of High Accuracy TVD Schemes for Hyperbolic Conservation Laws," AIAA Paper No. 85-0363, 1985.

[16]Roe, P. L., "Approximate Reimann Solvers, Parameter Vectors and Difference Scheme," *Journal of Computational Physics*, Vol. 43, 1981, pp. 357-372.

[17]Lu, P. J., Pan, D., and Yeh, D. Y., "On the Numerical Simulation of Trailing Edge Accoustic /Vortical Interaction," *AIAA Journal*, Vol. 33, No.5, May 1995, pp. 785-793.

[18]Lu, P. J., Pan, D., and Yeh, D. Y., "Transonic Flutter Suppression Using Active Accoustic Excitations," *AIAA Journal*, Vol. 33, No.5, April 1995, pp. 694-702.

[19]Venkatakrishnan, V., and Jameson, A., "Computation of Unsteady Transonic Flows by the Solution of Euler Equations," *AIAA Journal*, Vol. 26, No. 8, Aug. 1988, pp. 974-981.

[20]Thompson, K. W., "Time Dependent Boundary Conditions for Hyperbolic Systems," *Journal of Computational Physics*, Vol. 68, 1987, pp. 1-24.

[21]Hedstrom, G.W., "Nonreflecting Boundary Conditions for Nonlinear Hyperbolic Systems," *Journal of Computational Physics*, Vol. 30, 1979, pp. 222-237.

[22]Kinsler, L. E., Frey, A. R., Coppens, A. B. and Sanders, J.V., *Fundamentals of Acoustics*, Third Ed., Chapter 8, John Wiley and Sons, 1982.

[23]Ho, C. M., and Nosseir, N. S., "Dynamics of an Impinging Jet. Part I. The Feedback Phenomenon," *Journal of Fluid Mechanics*, Vol. 105,1981, pp. 119-142.

[24]Crighton, D. G., "The Excess Noise Field of Subsonic Jets," *Journal of Fluid Mechanics*, Vol. 56, 1972, pp. 683-694.

[25]Jou W. H. and Menon, S., "Modes of Oscillation in a Nonreacting Ramjet Combustor Flow," *AIAA Journal of Propulsion and Power*, Vol. 6, No. 5, 1990, pp. 535-543.

[26]Hankey, W.L. and Shang, J.S., "Analysis of Self-Excited Oscillations in Fluid Flows," AIAA Paper No. 80-1346, 1980.

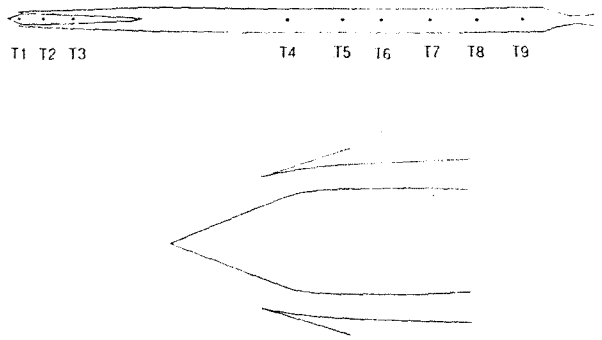

Fig. 1 Ramjet engine configuration and the pressure recording locations (T1 to T9).

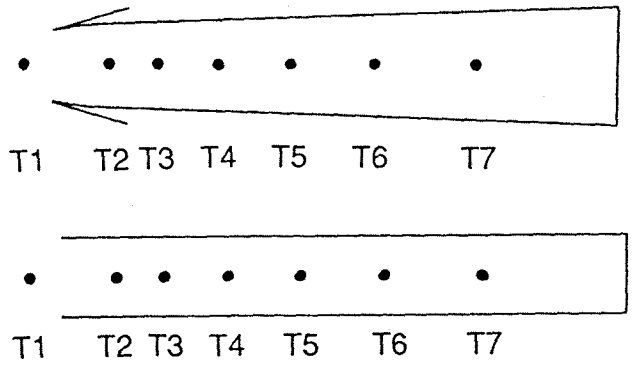

Fig. 2 A sketch of the Dailey's organ pipe and the constant cross-sectional pipe. Pressure histories are recorded at locations T1 to T7.

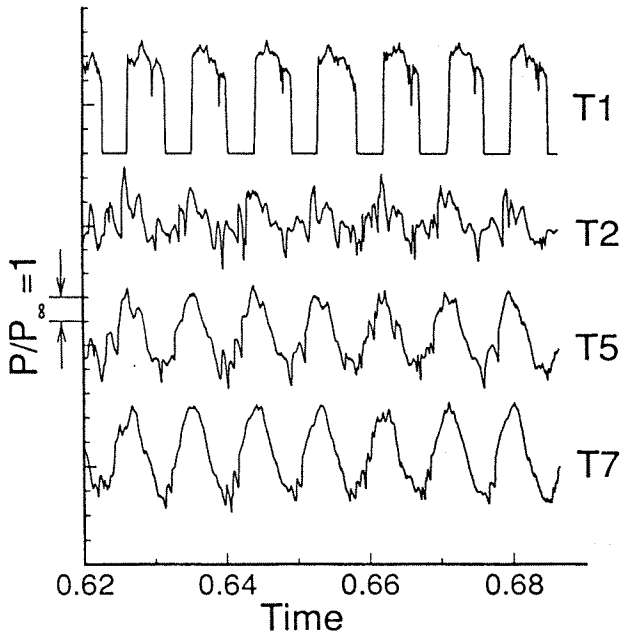

Fig. 3 Pressure histories recorded at T1,T2,T5 and T7. (Dailey's organ pipe).

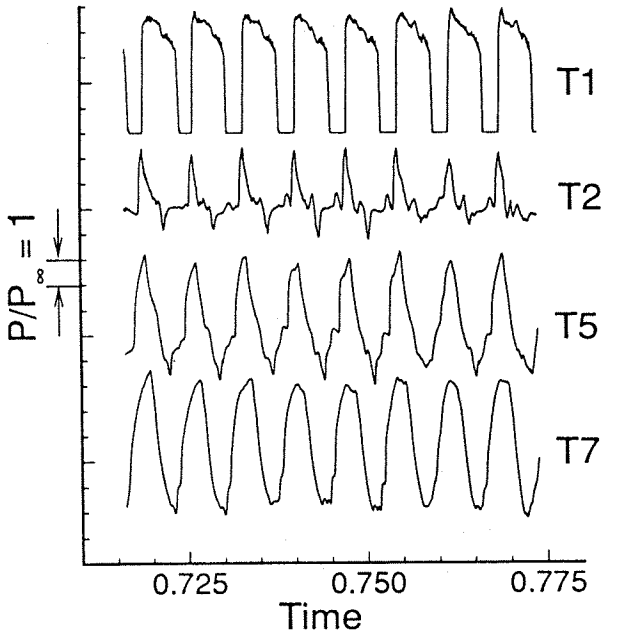

Fig. 4 Pressure histories recorded at T1, T2, T5 and T7. (constant cross-sectional pipe).

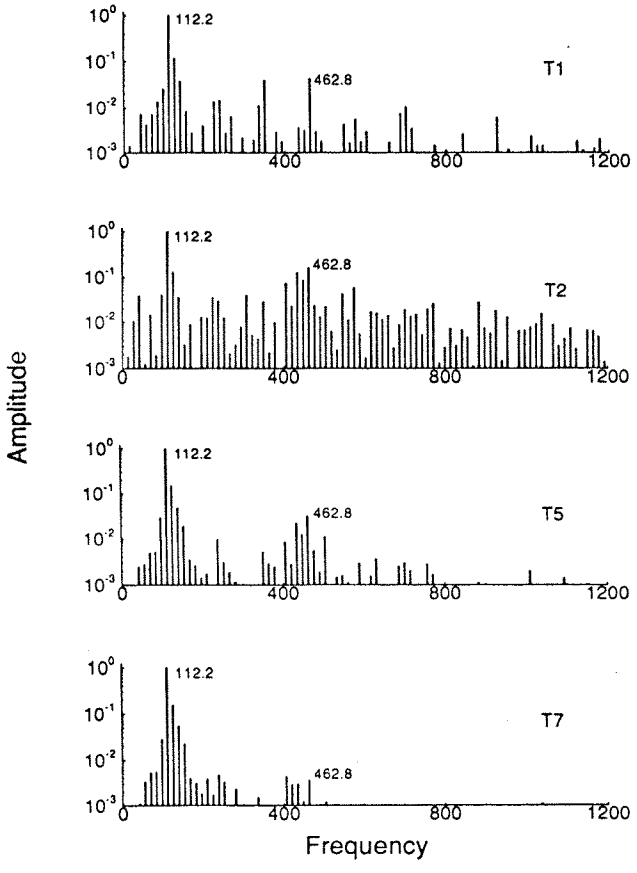

Fig. 5 The spectra of pressure histories recorded at T1, T2, T5, and T7. (Dailey's organ pipe).

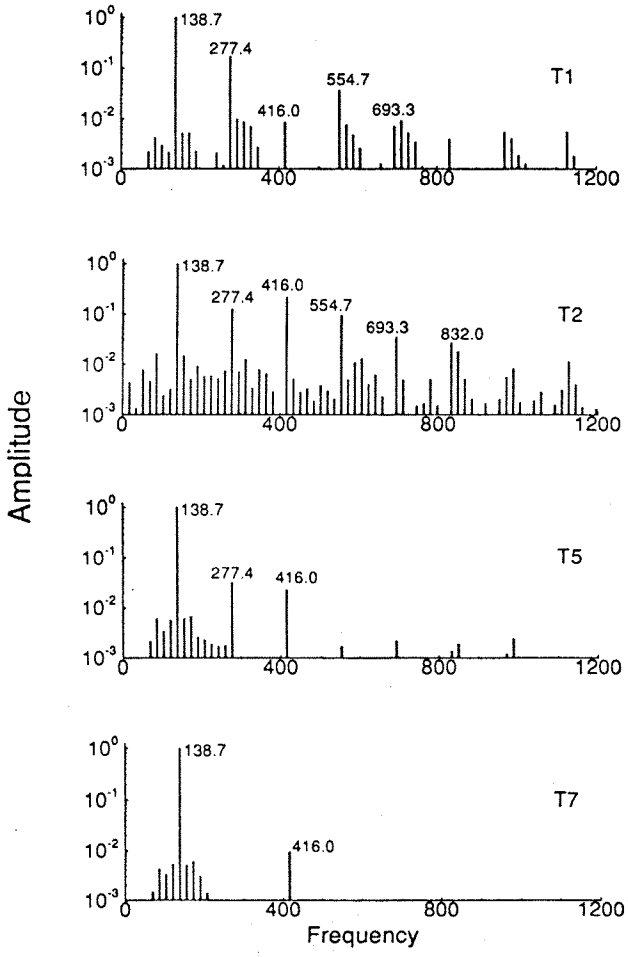

Fig. 6 The spectra of pressure histories recorded at T1, T2, T5, and T7. (constant cross-sectional pipe).

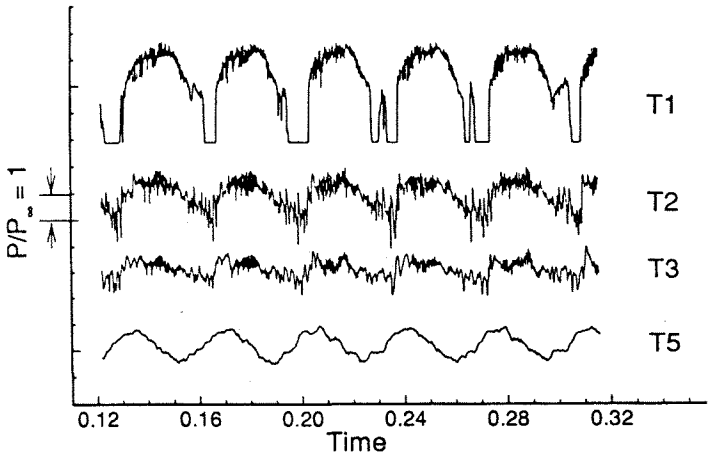

Fig. 7 Pressure histories recorded at four locations of a buzz simulation. (The first start-up case, engine length 10 ft).

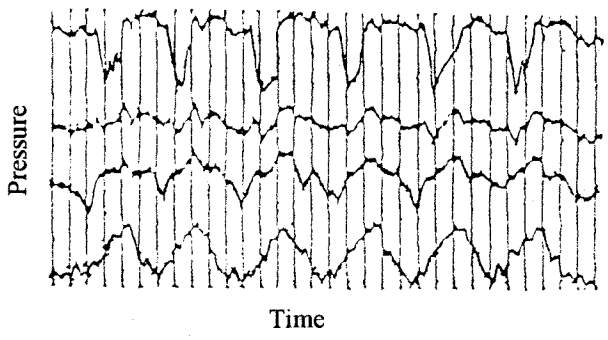

Fig. 9 Experimental pressure measurements during a buzz. (Picture adapted from Fig. 9 of Ref. 3).

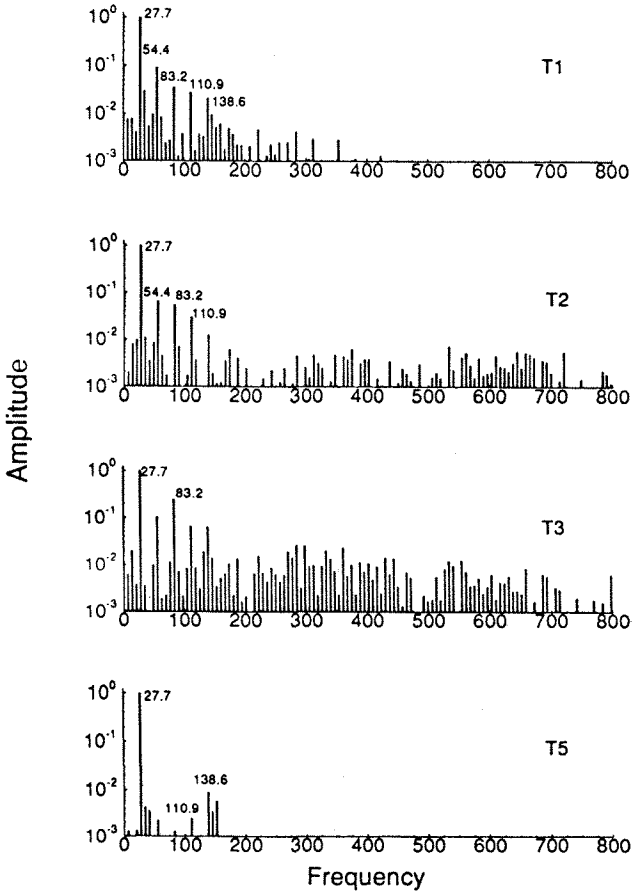

Fig. 8 The spectra of pressure histories recorded at T1, T2, T3, and T5. (The first start-up case, engine length 10 ft).

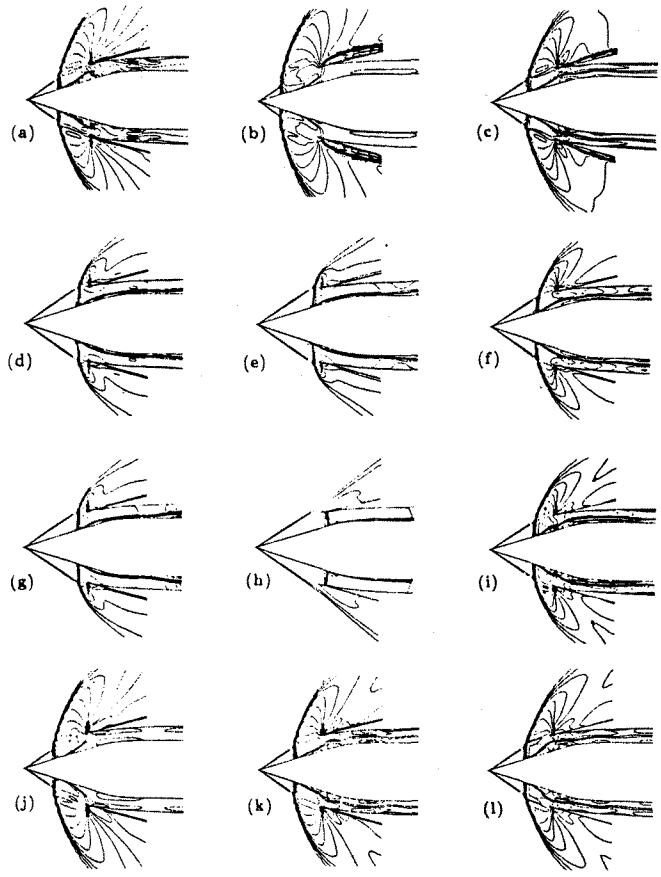

Fig. 10 Mach number contour plots in a buzz cycle.

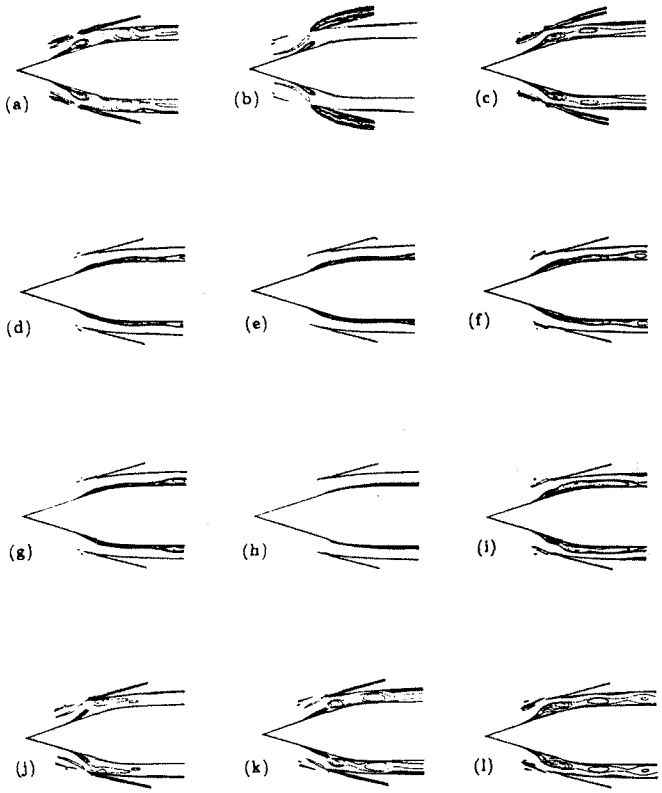

Fig. 11 Vorticiity contour plots in a buzz cycle.

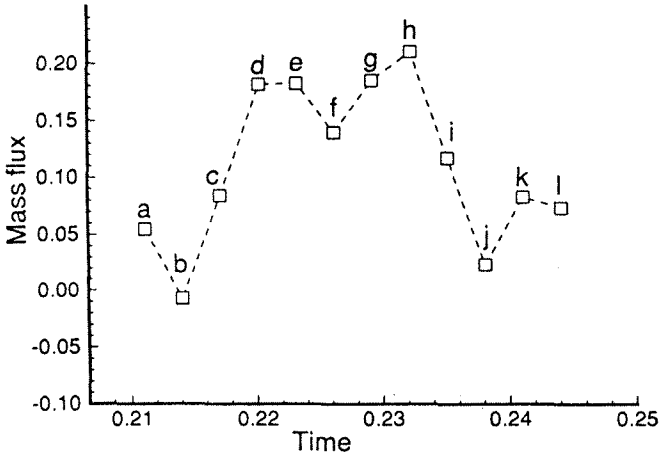

Fig. 13 The instantaneous mass fluxes at the entrance of the inlet in the selected twelve stages.

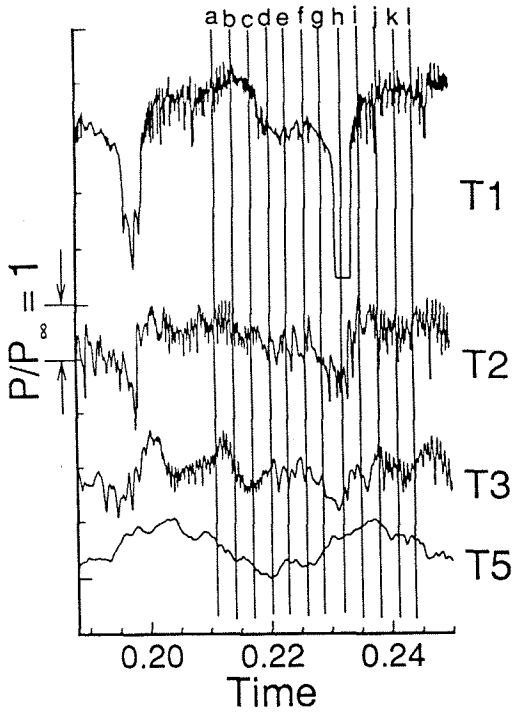

Fig. 12 Instants for snapshots to be taken in a buzz cycle.

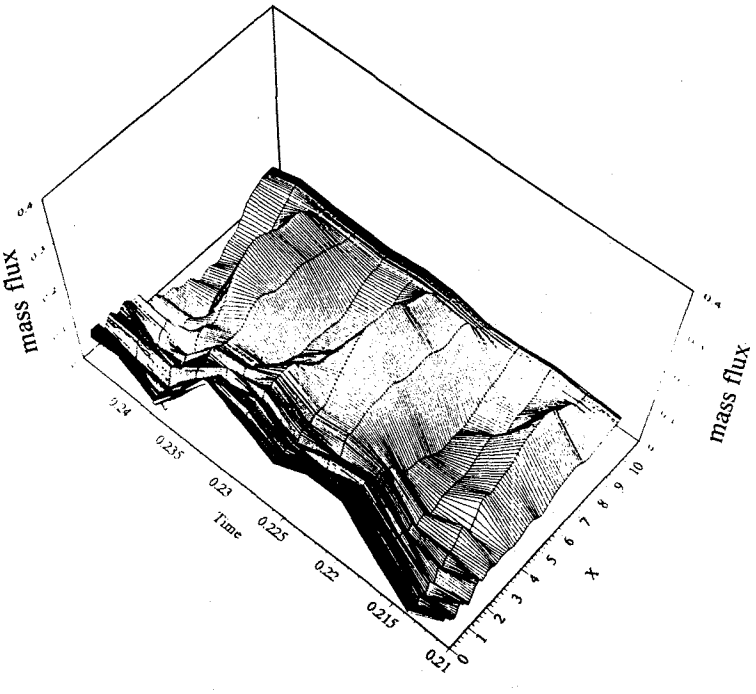

Fig. 14 The spatial-temporal mass flux distributions of the ramjet engine in a buzz cycle.

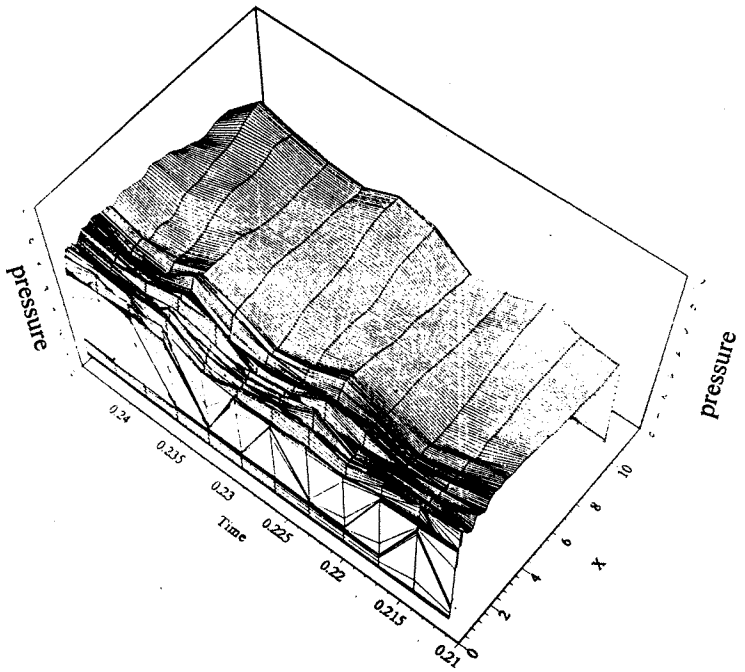

Fig. 15 The spatial-temporal pressure distributions of the ramjet engine in a buzz cycle.

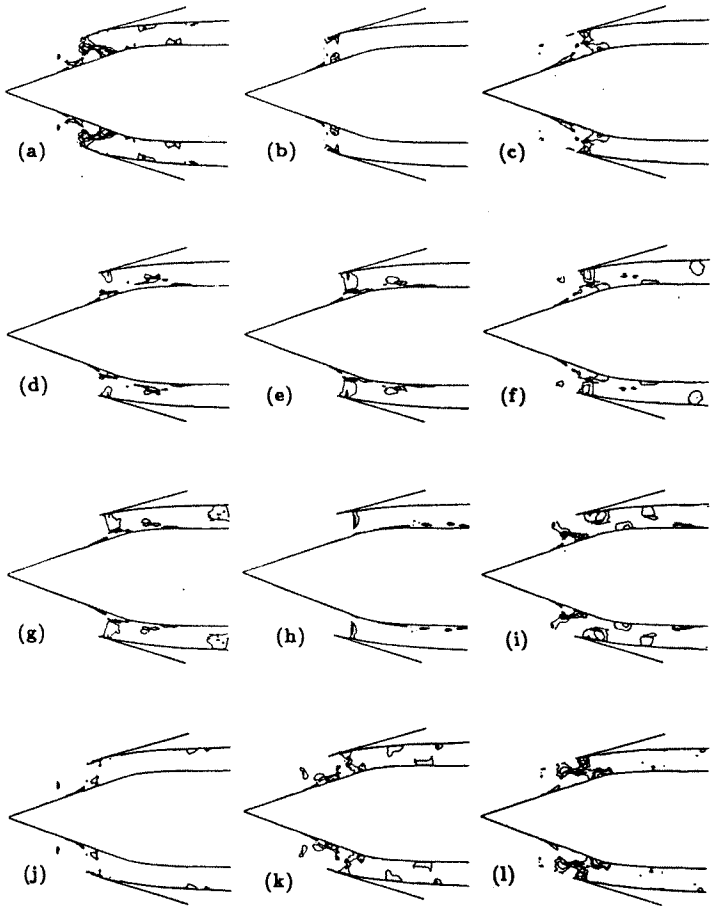

Fig. 16 Fluctuation dilatation fields during a buzz cycle.